bioRxiv preprint doi: https://doi.org/10.1101/2021.08.12.456011; this version posted October 29, 2021. The copyright holder for this preprint (which was not certified by peer review) is the author/funder, who has granted bioRxiv a license to display the preprint in perpetuity. It is made available under aCC-BY-NC-ND 4.0 International license.

Long reads and Hi-C sequencing illuminate the two compartment genome of the model arbuscular mycorrhizal symbiont *Rhizophagus irregularis*

Gokalp Yildirir [1*], Jana Sperschneider [2*], Mathu Malar C [1], Eric CH Chen [3], Wataru Iwasaki [3], Calvin Cornell [1] and Nicolas Corradi [1#]

[1] Department of Biology, University of Ottawa, ON, Ottawa, K1N 6N5, Canada

[2] Biological Data Science Institute, The Australian National University, Canberra, Australia

[3] Department of Integrated Biosciences, Graduate School of Frontier Sciences, The University of Tokyo, Japan

* contributed equally

Corresponding Author

Abstract

Chromosome folding links genome structure with gene function by generating distinct nuclear compartments and topologically associating domains (TADs). In mammals, these undergo preferential interactions and regulate gene expression. However, their role in fungal genome biology is unclear. Here, we combine Nanopore (ONT) sequencing with chromatin conformation capture sequencing (Hi-C) to reveal chromosome and epigenetic diversity in a group of obligate plant symbionts; the arbuscular mycorrhizal fungi (AMF). We find that five phylogenetically distinct strains of the model AMF *Rhizophagus irregularis* carry 33 chromosomes with substantial within species variability in size, as well as in gene and repeat content. Strain-specific Hi-C contact maps all reveal a 'checkerboard' pattern that underline two dominant euchromatin (A) and heterochromatin (B) compartments. Each compartment differs in the level of gene transcription, regulation of candidate effectors and methylation frequencies. The A-compartment is more gene-dense and contains most core genes, while the B-compartment is more repeat-rich and has higher rates of chromosomal rearrangement. While the B-compartment is transcriptionally repressed, it has significantly more secreted proteins and *in planta* up-regulated candidate effectors, suggesting a possible host-induced change in chromosome conformation. Overall, this study provides a fine-scale view into the genome biology and evolution of

bioRxiv preprint doi: https://doi.org/10.1101/2021.08.12.456011; this version posted October 29, 2021. The copyright holder for this preprint (which was not certified by peer review) is the author/funder, who has granted bioRxiv a license to display the preprint in perpetuity. It is made available under aCC-BY-NC-ND 4.0 International license.

prominent plant symbionts, and opens avenues to study the epigenetic mechanisms that modify chromosome folding during host-microbe interactions.

Introduction

Arbuscular mycorrhizal fungi (AMF) are obligate plant mutualistic organisms of the fungal subphylum Glomeromycotina (Spatafora *et al.*, 2016) that evolved a symbiotic relationship with the roots of most vascular plants species (Corradi & Bonfante, 2012; Martin *et al.*, 2017; Lutzoni *et al.*, 2018). During the AM symbiosis, these fungi enhance their host nutrient and water uptake in exchange of sugars and lipids, and provide an increased resistance against pathogens (Bonfante & Anca, 2009). The first fossil records of the AM symbiosis date several hundred million years, and today this symbiotic relationship between AMF and their plant hosts is widespread globally, highlighting AMF's capacity to persist in various environmental conditions (Delaux & Schornack, 2021). AMF spores and hyphae harbor up to thousands of coexisting nuclei at all times (Kokkoris *et al.*, 2020), and their genetics are defined by the presence of two life stages – i.e. the homokaryotic stage (AMF homokaryons), where co-existing nuclei are genetically largely uniform, and the heterokaryotic stage (AMF dikaryons), where nuclei originating from two parental strains coexist in the mycelium (Ropars *et al.*, 2016; Corradi & Brachmann, 2017; Chen *et al.*, 2018a; Kokkoris *et al.*, 2021).

Genome analyses revealed that species in the Glomeromycotina carry gene losses in cellular pathways that inhibit the metabolism of fatty acids, sugars and plant cell wall degradation enzymes (Tisserant et al., 2013; Lin et al., 2014; Chen et al., 2018b; Morin et al., 2019; Malar C et al., 2021a), and contain an abundance of transposable elements (TE). Closely related AMF strains also vary dramatically in their gene content, suggesting that AMF have pangenomes (Chen *et al.*, 2018b; Mathieu *et al.*, 2018a). The pangenome concept highlights the distinction between 'core' conserved genes hypothesized to be essential for daily activities (e.g. cytoskeleton, protein translation, etc.), and 'dispensable' non-conserved genes thought to help individual strains adapt to changing environments and hosts (e.g. transduction signalling, effectors, etc.) (Li *et al.*, 2018; McCarthy & Fitzpatrick, 2019; Badet *et al.*, 2020) (Li *et al.*, 2018; McCarthy & Fitzpatrick, 2019; Badet *et al.*, 2020).

Identifying the mechanisms from which pangenomes emerge is essential for understanding the mode of evolution of these widespread plant symbionts. In fungal plant pathogens, high repeat

bioRxiv preprint doi: https://doi.org/10.1101/2021.08.12.456011; this version posted October 29, 2021. The copyright holder for this preprint (which was not certified by peer review) is the author/funder, who has granted bioRxiv a license to display the preprint in perpetuity. It is made available under aCC-BY-NC-ND 4.0 International license.

content generates within-species genome variability and it was proposed that similar mechanisms drive genetic variability in AMF (Chen *et al.*, 2018b; Mathieu *et al.*, 2018a). However, this hypothesis is currently untestable for AMF because most available genome assemblies are highly fragmented – i.e. composed in many cases of dozens of thousands of contigs (Chen *et al.*, 2018b; Mathieu *et al.*, 2018b). This high fragmentation rate can generate mosaic sequences of multiple haplotypes (collapsed regions), chimeric assemblies and artificial gene duplications (Denton *et al.*, 2014; Montoliu-Nerin *et al.*, 2020), preventing fine-scale and reliable analyses of genome rearrangements, repeat diversity, and repeat plasticity within and across strains.

The highly fragmented state of AMF genomes also hampered the identification of mechanisms that define relationships between genome structure and function. Within nuclei, chromosomes separate into two groups: active open chromatin A-compartments (euchromatin) and less active chromatin B-compartments (heterochromatin) and each compartment can be differently regulated (Pombo & Dillon, 2015; Dekker & Heard, 2015; Szabo *et al.*, 2019; Kempfer & Pombo, 2020). This compartment-driven gene regulation highlights the key epigenetic role of chromosome folding for genome biology, but knowledge of this process in fungi was thus far restricted to a few model genera (e.g. *Sacharomyces*, *Neurospora*) and the filamentous fungus *Epichloë festucae* (Galazka *et al.*, 2016; Kim *et al.*, 2017; Winter *et al.*, 2018).

In the plant symbiont *E. festucae*, chromosome folding and repetitive elements together divide the genome into distinct regions with very similar gene expression suggesting that both genome characteristics co-regulate symbiotic associations in this species. However, whether similar mechanisms drive gene expression and symbiotic associations in other fungal symbionts, including AMF, is unknown. Here, we aimed to obtain a complete understanding of the AMF genome biology and within species genome dynamics by acquiring long-read and strain-specific high-throughput chromatin conformation capture (Hi-C) sequencing data (Schmitt *et al.*, 2016) from five phylogenetically distinct homokaryotic strains of the species *R. irregularis*.

Materials and Methods

Culturing, DNA Extraction and ONT/Hi-C Sequencing

R. irregularis strains A1 (DAOM-664342), B3 (DAOM-664345) and C2 (DAOM-664346) were originally isolated from Switzerland (Tänikon), while the strain DAOM-197198 was originally isolated from Pont Rouge, Canada (Koch *et al.*, 2004; Stockinger *et al.*, 2009) and the strain

bioRxiv preprint doi: https://doi.org/10.1101/2021.08.12.456011; this version posted October 29, 2021. The copyright holder for this preprint (which was not certified by peer review) is the author/funder, who has granted bioRxiv a license to display the preprint in perpetuity. It is made available under aCC-BY-NC-ND 4.0 International license.

4401 (DAOM-240446) was isolated from *Ammophila breviligulata* in "La Martinique Îles-de-la-Madeleine" (Canada).

All five strains were cultured *in vivo*, using *Daucus carota* root organ cultures (ROCs) as the host, as previously described (Corradi *et al.*, 2004). The strains propagated in two-compartment ROCs, allowing us to produce mycelium and spores without obvious contaminants. For Oxford Nanopore (ONT) sequencing, high quality, high molecular weight DNA was extracted for the strains A1, C2, B3 and 4401 using a protocol proposed by Schwessinger (Schwessinger, 2016). Following extraction, high quality DNA samples were processed using Nanopore Ligation Sequencing Kit SQK-LSK109 to prepare the sequencing libraries, which were sequenced using the MinION R9.4.1 flowcells to produce an average of 8.45 million reads with an N50 > 4Kb, reaching to a genome coverage of 160x.

Chromosome assembly and annotation

ONT reads were basecalled with guppy (version 4.5.2) using the "high accuracy" configuration (dna_r9.4.1_450bps_hac.cfg), and were used to generate assemblies using Canu (version 2.0) (Koren *et al.*, 2017). These assemblies were then further polished using Racon (v 1.4.10) (Vaser *et al.*, 2017) using the default parameters and the consensus sequences were created using Medaka (version 1.0.3). The polishing step was concluded with two rounds of Pilon (version 1.23) using Illumina reads and default parameters (Walker *et al.*, 2014). Illumina reads were then mapped on the polished contigs using bwa mem (version 0.7.17) (Li, 2013) and the read coverage of each contig was calculated using bedtools (version 2.26.0) (Quinlan & Hall, 2010). Contigs having abnormally low (<5x) and high (>200x) coverages were filtered out using purge_haplotigs (Roach *et al.*, 2018), and the remaining contigs were used for further scaffolding. Illumina reads used for polishing from the strains A1, B3 and C2 were obtained from Ropars *et al.* (Ropars *et al.*, 2016), DAOM197198 reads were obtained from Chen et al. 2018(Chen *et al.*, 2018b), 4401 Illumina reads were used in this study for the first time.

Approximately 200 mg of fresh mycelium from each strain was crosslinked and shipped to Phase Genomics (Seattle, WA) to obtain strain-specific Hi-C data. Hi-C data was produced using the Proximo Hi-C Kit (Microbe) at the Phase Genomics with DPNII restriction enzymes. Before generating high-throughput Hi-C Illumina data, the quality of these libraries was assessed by mapping a low coverage paired-end data onto available *R. irregularis* assemblies. A library is

bioRxiv preprint doi: https://doi.org/10.1101/2021.08.12.456011; this version posted October 29, 2021. The copyright holder for this preprint (which was not certified by peer review) is the author/funder, who has granted bioRxiv a license to display the preprint in perpetuity. It is made available under aCC-BY-NC-ND 4.0 International license.

deemed to be of high quality if the fraction of high quality paired-end reads mapping respectively > 10KB apart within and across publicly available contigs exceeds 1.5% and 5.0%. In all cases, the values obtained for our samples far exceeded the QC limits set by Phase Genomics (Seattle, WA) – e.g. average 11.75% and 23%.

The subsequent Illumina library preparation and sequencing yielded paired-end Hi-C reads of 150 bp at 75x-150x coverage. Scaffolding was carried out with contigs that were obtained using Canu and strain-specific Hi-C data. For scaffolding, the Hi-C reads were first mapped to each contig using BWA-MEM 0.7.17 (Li, 2013). Alignments were then processed with the Arima Genomics pipeline (Arima Genomics, 2019). Scaffolding was performed using SALSA 2.2 (Ghurye *et al.*, 2017, 2019) and subsequent manual curation was guided by Hi-C contact maps. For strain C2, SALSA scaffolding resulted in 202 scaffolds from 325 contigs and 15 contigs were broken based on Hi-C contact map information. For strain A1, SALSA resulted in 107 scaffolds from 276 contigs and 14 contigs were broken based on Hi-C contact map information. For strain 4401, SALSA resulted in 108 scaffolds from 306 contigs and 13 contigs were broken based on Hi-C contact map information. For strain B3, SALSA resulted in 138 scaffolds from 314 contigs and 13 contigs were broken based on Hi-C contact map information. In the strain DAOM-197198 SALSA resulted in 153 scaffolds from 210 contigs, and one contig was broken based on Hi-C contact map information.

Gene annotation was achieved by using Funannotate (version 1.7.4) (https://zenodo.org/record/2604804#.YPm336iSnIU) on repeat-masked genome assemblies. Genome annotations were performed using RNA-seq reads and protein models for the strains DAOM197198, A1, B3 and C2 available from the Joint Genome Institute (JGI; (Chen *et al.*, 2018b)). For the strain 4401, genome annotation was carried by combining EST, RNA-seq and models from the strains DAOM197198, C2 and B3. The quality of annotations was evaluated using the Benchmarking Universal Single-Copy Orthologs (version 4.0, database Obd_10) (Simão *et al.*, 2015).

Conserved protein domains were predicted using Pfam v.27 (El-Gebali *et al.*, 2019). SignalP 4.1 (-t euk -u 0.34 -U 0.34)(Petersen *et al.*, 2011) and TMHMM 2.0(Krogh *et al.*, 2001) were used to predict secreted proteins. A protein was called secreted if it was predicted to have a signal peptide and but no transmembrane domains. Effector candidates were predicted with EffectorP

bioRxiv preprint doi: https://doi.org/10.1101/2021.08.12.456011; this version posted October 29, 2021. The copyright holder for this preprint (which was not certified by peer review) is the author/funder, who has granted bioRxiv a license to display the preprint in perpetuity. It is made available under aCC-BY-NC-ND 4.0 International license.

3.0(Sperschneider & Dodds, 2021). De novo repeats were predicted with RepeatModeler 2.0.0 and the option -LTRStruct (Flynn *et al.*, 2020). These were merged with the RepeatMasker repeat library and RepeatMasker 4.1.0 was run with this combined repeat database (Smit *et al.*). Transposable element locations were extracted from the Repeatmasker output file using an R script and simple repeats, unknown and low complexity repeats, satellites, tRNA, snRNA and rRNAs were filtered out from the output file. PfamScan (Hancock & Bishop, 2004; Li *et al.*, 2015) was used with default parameters to identify the protein domain annotations in all strains. To create the Pfam heatmaps, the domain numbers were counted for each *R. irregularis* strain or A/B compartment, and a t-test conversion was made to highlight the protein domain abundances for each category.

We used mash dist (version 2.2.0) (Ondov *et al.*, 2016) for *k-mer* distance calculations and dnadiff from the MUMmer (Kurtz *et al.*, 2004; Marçais *et al.*, 2018) suite for structural variation calculations between strains and compartments. Orthology analyses were made by FastOrtho (Wattam *et al.*, 2014), using following parameters: 50% identity and 50% coverage using protein sequences of all five assemblies. All karyoplots were produced using KaryoploteR (Gel & Serra, 2017). All genome data and reads newly obtained are available in Genbank under the BioProject PRJNA748024.

Identification of chromosome compartments and topologically associated domains

We called A/B compartments and TADs with hicexplorer 3.6 (Ramírez *et al.*, 2018) using the commands hicPCA and hicFindTADs, respectively. Inter- and intra-chromosomal Hi-C contact maps were produced with HiC-Pro 2.11.1 (Servant *et al.*, 2015) (MAPQ=10) and hicexplorer 3.6 (Ramírez *et al.*, 2018; Wolff *et al.*, 2018, 2020; Winter *et al.*, 2018) and these Hi-C contact maps were manually inspected to assign chromosomal regions to A/B compartments. Specifically, the regions along the each chromosomes carrying the same PCA1 values – i.e. positive or negative – were assigned to the same compartment. Following this assignment, compartments were manually inspected to investigate their proximity with other chromosomes. Those in close physical proximity with the smallest chromosomes were assigned to compartment A, while those carrying the counterpart PCA1 signal were assigned to compartment B. This process was manually repeated for all 33 chromosomes individually to separate the chromosomal

bioRxiv preprint doi: https://doi.org/10.1101/2021.08.12.456011; this version posted October 29, 2021. The copyright holder for this preprint (which was not certified by peer review) is the author/funder, who has granted bioRxiv a license to display the preprint in perpetuity. It is made available under aCC-BY-NC-ND 4.0 International license.

regions into separate A/B compartments. Bedtools (Quinlan & Hall, 2010) was used to assess overlap between genomic features such as genes/repeats and compartments.

Methylation and gene expression analyses

Megalodon (version 2.2.9) was used for methylation calling using the high accuracy parameters (dna_r9.4.1_450bps_modbases_dam-dcm-cpg_hac.cfg) configuration file. After methylation calling was completed for all five assemblies, CG positions and their methylation frequencies were extracted from the 5mC bedfile output. For RNA-seq analyses, Salmon v.1.3.0 (Patro *et al.*, 2017) was used to align clean RNA-seq reads to the transcripts and to estimate transcript abundances in each sample (salmon index –keepDuplicates and salmon quant –validateMappings). We used tximport and DESeq2 (Love *et al.*, 2014) to assess gene differential expression (padj < 0.1). The DAOM-197198 RNA-seq datasets used in this study were obtained from germinating spores (SRR1979300-SRR1979302), as well as intra-radical material isolated from *Medicago Trunculata* (SRR5644319-SRR5644324) and *Allium schoenopasum* (SRR5644331- SRR5644333).

Results

Assembly and annotation of Rhizophagus irregularis chromosomes

Basecalled and polished ONT data from four homokaryotic strains (A1, B3, C2 and 4401) were assembled using Canu (Koren *et al.*, 2017), and then scaffolded using strain-specific Hi-C data. The same scaffolding procedures were performed on a previously published PacBio assembly of the model AMF strain DAOM197198 (Maeda *et al.*, 2018). This approach resulted in an average of 137 scaffolds with an N50 score of 5 Mb, which were further curated into 33 chromosome-scale scaffolds in each strain, guided by Hi-C contact maps (**Table 1, Figure S1**).

When combining the five strains, we found telomeres on both ends for 32 of the 33 chromosomes (only chromosome 2 has telomeres on only one end in all strains). Genome sizes are very similar in the model strain DAOM197198, A1, B3 and 4401 at 146-147 Mb, while the C2 strain harbors a larger genome at 162 Mb, consistent with published flow cytometry analyses (Ropars *et al.*, 2016). For all five strains, the number of unplaced contigs is small (12-104 contigs at size 0.4-2.6 Mb) and all unplaced contigs are short indicating that the chromosome assemblies are near-complete (**Table 1, Figure S1**).

bioRxiv preprint doi: https://doi.org/10.1101/2021.08.12.456011; this version posted October 29, 2021. The copyright holder for this preprint (which was not certified by peer review) is the author/funder, who has granted bioRxiv a license to display the preprint in perpetuity. It is made available under aCC-BY-NC-ND 4.0 International license.

We identified an average of 76 families of repeats and known transposable elements (TE) encompassing on average 50.2% of the genome (**Figure S2**). When only TEs are considered, repeat density varies across chromosomes of different strains. For DAOM197198, A1 and B3 assemblies, chromosome 2 has the highest TE density (17.2%, 14.8% and 14.8% respectively), whereas the highest TE density is chromosome 33 for the C2 assembly (20.8%), and chromosome 23 for the 4401 assembly (15.6%). The chromosome with the lowest TE density is chromosome 20 for A1 and B3 (8.5% and 9.4%, respectively), chromosome 28 for DAOM197198 (9.2%), chromosome 3 for C2 (11.9%) and chromosome 8 for 4401 (7.3%).

Gene annotation identified between 23,693 to 26,820 genes, in line with past work based on fragmented datasets (Chen *et al.*, 2018b), and BUSCO completeness averages 96% (**Table 1**). Gene density varies among chromosomes, with chromosome 32 always having the highest density while chromosome 15 the lowest (**Figure S1**). A hallmark of AMF is that they carry divergent rRNA operons within their genome. In DAOM197198 one rRNA operon is found on chromosome 9, two operons co-locate on chromosomes 23 and 28, and five are present in chromosome 18 (**Figure S1)**. The putative AMF mating-type locus (Ropars *et al.*, 2016) is located on chromosome 11 in all strains (**Figure S1**).

Within species chromosome diversity in R. irregularis

Consistent with previous reports on fragmented assemblies (Chen et al., 2018b), the *R. irregularis* gene content is divided into genes shared by all strains (core genes) and genes shared by only a few strains or strain-specific (dispensable) (**Figure S3a**), and on average only 55.8% of *R. irregularis* genes are core (Chen *et al.*, 2018b). Our analyses confirm that within species variability affects the number of rRNA operons (**Figure 1a**, **Table S1**) (Corradi *et al.*, 2007), and each strain carries a distinct abundance of protein domains (**Figure S3b**) (Chen *et al.*, 2018b).

Homologous chromosomes often differ in size between strains. For example, the largest chromosome of the 4401 strain is chromosome 8 at 6.3 MB in size but this chromosome is only 5.2 MB in DAOM197198 (**Figure 1b**). The chromosome with the putative MAT-locus (Chromosome 11) varies in size from a maximum of 5.6 Mb in C2 to a minimum of 5 Mb in 4401, even though they carry the same mating type (**Figure 1c**). We used a *k*-mer distance measure to assess relatedness of strains and their chromosomes. Overall, the strain DAOM197198 is related to the strain 4401, strains B3 and A1 are related, and C2 is the most

bioRxiv preprint doi: https://doi.org/10.1101/2021.08.12.456011; this version posted October 29, 2021. The copyright holder for this preprint (which was not certified by peer review) is the author/funder, who has granted bioRxiv a license to display the preprint in perpetuity. It is made available under aCC-BY-NC-ND 4.0 International license.

distant (**Figure S4**). However, this is not consistent across all chromosomes. For example, chromosome 8 shows higher levels of similarity between strain DAOM197198 and the strains B3 and A1 while chromosome 25 shows higher levels of similarity between strain 4401 and the strains B3 and A1 (**Figure S4**). These results support past reports of phylogenetic incongruence and inter-strain genetic exchange in *R. irregularis* (Riley *et al.*, 2014; Chen *et al.*, 2018b)**.**

The chromosomes of Rhizophagus irregularis form a two-compartment genome

Hi-C sequencing also generated direct, quantitative evidence of the 3D nuclear organization in five *R. irregularis* strains. For the strains DAOM197198, A1 and C2, this revealed that chromosomes form a distinct 'checkerboard' pattern that defines the long-range interactions that form two nuclear A/B compartments in eukaryotes, including fungi (Fortin & Hansen, 2015; Kim *et al.*, 2017; Spielmann *et al.*, 2018; Winter *et al.*, 2018; Falk *et al.*, 2019) (Figure 2, **Figures S5-10**).

In the model strain DAOM197198, the A-compartment has a total size of 58.1 Mb while B-compartment is 73.5 Mb, and respectively each contains 96 and 83 TADs. Chromosome varies in the degree of compartmentalization – e.g. chromosome 2 has consistent swaps between A- and B-compartment, while the A-compartment dominates in the smallest chromosomes (chr30 – 33) **(Figure S6-10)**. Although *Rhizophagus irregularis* Hi-C contact maps did not show easily recognizable centromere hotspots found in rust fungi (Sperschneider *et al.*, 2021), these reveal telomere-to-telomere interactions that define all chromosomes boundaries and confirm our assembly. Changes in Hi-C contacts between homologous chromosomes of different strains are also linked with the emergence of large strain-specific repeat and gene expansions (**Figure S11a**), or inversions (**Figure S11b,c,d**).

In the model strain DAOM197198, the A-compartment is more gene dense with 2.55 genes and 18.21 repeats per 10 Kb, while the B-compartment carries an average of 1.74 genes and 18.9 repeats per 10 Kb (**Figure 3a, Table S2)**. The A-compartment also codes for 90% of BUSCO proteins, and double the number of core genes (**Figure S12**), while B-compartment carries most dispensable genes and many highly expanded families – e.g. Tyrosine Kinases, the tetratricopeptide repeat Sel-1, the homodimerization BTB. The large high mobility box (HMG) gene family is, however, predominant in the B-compartment (**Figure 3b**). Remarkably, while the B-compartment is less gene-dense, it is enriched for predicted secreted proteins as well as for

bioRxiv preprint doi: https://doi.org/10.1101/2021.08.12.456011; this version posted October 29, 2021. The copyright holder for this preprint (which was not certified by peer review) is the author/funder, who has granted bioRxiv a license to display the preprint in perpetuity. It is made available under aCC-BY-NC-ND 4.0 International license.

candidate apoplastic and cytoplasmic effectors and carries the cytoplasmic *R. irregularis* effector SP7 on chromosome 1 (Kloppholz *et al.*, 2011).

We hypothesized that the distinct gene and repeat densities result in different structural rearrangement rates between A/B compartments. We measured the degree of structural variation and sequence identity of each compartment, and found that the sequence alignments between strains in the B-compartment are shorter and have lower sequence identity than sequence alignments in the A-compartment. The B-compartment also contains more structural variation (**Table S3**, **Figure S13**).

Gene expression and methylation in chromosomal compartments

In other organisms, euchromatin (A compartments) is generally transcriptionally active while heterochromatin (B compartments) are repressed (Szabo *et al.*, 2019; Zheng & Xie, 2019; Jerković *et al.*, 2020). To test if this dichotomy also applies to AMF, we investigated gene expression between compartments in DAOM197108 using three high quality RNA-seq datasets obtained from intra-radical hyphae in symbiosis with *Allium*, arbuscocytes in symbiosis with *Medicago* and germinating spores (Kamel *et al.*, 2017; Zeng *et al.*, 2018).

In *R. irregularis*, genes in the A compartment have, on average, significantly higher expression levels than those in the B compartment (**Figure 4a**). However, this compartment also has lower expression levels in the *in planta* conditions (*Allium*: 57.3 TPMs; *Medicago*: 56 TPMs) than in germinated spores (62.4 TPMs). Remarkably, the inverse pattern is observed for genes in the B-compartments, which have higher expression levels in the *in planta* conditions (*Allium*: 16.8 TPMs; *Medicago*: 19.5 TPMs) than in germinated spores (11.2 TPMs), and genes encoding secreted proteins are significantly up-regulated in both *in planta* conditions in the B-compartment, but not in the A-compartment (**Figure 4b**). We also aimed to investigate the expression of these regions within TAD, and found that genes tend to be co-regulated when they are located in the same TAD in the A-compartment, while co-regulation within the same TAD was not observed for the B-compartment **(Figure S14)**.

We used ONT sequencing to call methylated sites and test if the difference in the A/B compartment gene expression resulted from different methylation patterns (Lea *et al.*, 2018; Dallaire, 2021). In DAOM197198 strain, CG dinucleotides are highly enriched for 5mC methylation – i.e. 11.88% for CG compared to 0.72 to 3.95% for other dinucleotides contexts

bioRxiv preprint doi: https://doi.org/10.1101/2021.08.12.456011; this version posted October 29, 2021. The copyright holder for this preprint (which was not certified by peer review) is the author/funder, who has granted bioRxiv a license to display the preprint in perpetuity. It is made available under aCC-BY-NC-ND 4.0 International license.

(CA, CC, CT) – 6mA methylation is very low regardless of dinucleotide contexts (AA, AC, AG, AT: 0.01% to 0.06). This indicates that 5mC methylation in the CG dinucleotide context is the primary DNA methylation process active in this species.

Overall, the CpG sites are significantly more methylated in the A-compartment, particularly for highly methylated sites (methylation frequency > 80%) (**Figure S13a)**. Within the B compartment, 22.5% of all protein encoding genes are highly methylated compared to 18.4% in the A-compartment (**Figure 4c**). When TEs are considered, this is inversed with 67% of methylated TEs families (24 out of 35) being highly methylated in the A-compartment compared to only 25% for the B -compartment (9 out of 36) (**Figure S13b**). Among TEs that are compartment specific - e.g Ginger DNA 2, DNA Zisupton and LINE Penelope are only found in compartment B and the LINE -Tad, and LINE R1-LOA carried by the A-compartment – only those located in the A-compartment are methylated.

Discussion

A chromosome-level view of a model AMF pangenome

The present study confirms that the combined number of genes within the model AMF *R. irregularis* far exceeds that found in individual strains (Chen *et al.*, 2018b; Mathieu *et al.*, 2018b; Reinhardt *et al.*, 2021). It also revealed that strains in this model species carry 33 homologous chromosomes (possibly the largest number identified in a fungus) and within-species variability in chromosome size and epigenetics (folding and methylation).

Size difference among homologous chromosomes affects all strains, regardless of their phylogenetic clustering (Savary *et al.*, 2018; Chen *et al.*, 2018b; Kokkoris *et al.*, 2021) or MAT-locus identity – e.g. strains C2 and 4401 carry the MAT-locus-6 (as defined by (Ropars *et al.*, 2016)) on chromosome 11 but this chromosome is 640 Kb larger in C2 compared to 4401. Despite this variability, all strains analysed carry the same number of homologous chromosomes, and future studies may reveal if this characteristic defines species boundaries in this taxonomically challenging taxon (Bruns *et al.*, 2018).

Chromosome compartments dictate AMF genome biology and evolution

Hi-C data revealed that AMF chromosomes separate into locations with euchromatin (transcriptionally active A-compartment) and heterochromatin (transcriptionally less active B-

bioRxiv preprint doi: https://doi.org/10.1101/2021.08.12.456011; this version posted October 29, 2021. The copyright holder for this preprint (which was not certified by peer review) is the author/funder, who has granted bioRxiv a license to display the preprint in perpetuity. It is made available under aCC-BY-NC-ND 4.0 International license.

compartments) that regulate both the expression and evolution of distinct molecular functions. In the A-compartment, higher gene density and repeat methylation indicates a tighter control of repeat expansions that could be deleterious for a region that contain most core genes. In contrast, the B-compartment experiences higher gene and lower repeat methylation rates, which explains its reduced gene expression levels and higher rearrangement rates.

It was proposed that AMF and notorious plant pathogens (e.g. *Fusarium oxysporum*, *Verticillium dahlia*; *Zymoseptoria tritici*) evolved similar genomic strategies to cope with their evolving plant hosts and competitors (Reinhardt *et al.*, 2021). The A/B compartments are reminiscent of the "two-speed genome architecture" reported in some fungal plant pathogens, where highly repetitive and rapidly rearranging genomic regions that express secreted proteins (i.e. analogous to B-compartments) separate from gene-rich locations that carry most core genes (i.e. analogous to A-compartments) (Mathieu *et al.*, 2018a). Another similarity with plant pathogens is the presence in *R. irregularis* strains of many dispensable and lineage-specific genes. Despite this genomic resemblance, however, our analyses did not reveal the presence in *R. irregularis* of dispensable chromosomes that drive the adaptation of fungal plant pathogens to changing environments (Garmaroodi & Taga, 2007; Vlaardingerbroek *et al.*, 2016; Bertazzoni *et al.*, 2018).

A role of a two-compartment genome in plant colonization?

We showed that the A/B compartments have distinct epigenetic signatures, and in line with mammalian studies, the A-compartment in *R. irregularis* is transcriptionally active whereas the B-compartment is repressed. However, we also found that this does not hold true for genes encoding secreted proteins and candidate effectors. During two *in planta* conditions, we observed increased up-regulation of genes encoding secreted proteins in the B-compartment, but not in the A-compartment. This suggests that the repressed state of the B-compartment might be relaxed during plant colonization, possibly induced through signals from the plants (Plett & Martin, 2012). In the fungal pathogen *Leptosphaeria maculans* epigenetic control mechanisms lead to effector gene regulation (Soyer *et al.*, 2014). As our Hi-C data derives from extraradical mycelium, acquiring similar data *in planta* may show that intra-radical mycelium carries distinct chromosome conformations that lift repression for the *R. irregularis* B-compartment (Frantzeskakis *et al.*, 2019; Torres *et al.*, 2020).

bioRxiv preprint doi: https://doi.org/10.1101/2021.08.12.456011; this version posted October 29, 2021. The copyright holder for this preprint (which was not certified by peer review) is the author/funder, who has granted bioRxiv a license to display the preprint in perpetuity. It is made available under aCC-BY-NC-ND 4.0 International license.

Conclusions

Combining long-reads with Hi-C sequencing demonstrates that model arbuscular mycorrhizal symbionts all carry 33 chromosomes with contents and sizes that varies significantly among strains. This supports the notion that AMF have pangenomes and, more generally, that conspecific strains should never be assumed to have identical genomes and genes (Malar C *et al.*, 2021b).

Our work also uncovered a higher-order genome organization that governs AMF genome biology and evolution. Dispensable genes and the most expressed and regulated secreted proteins - i.e. those potentially involved in the molecular dialogue with the plant hosts - locate primarily in the rapidly evolving B-compartments, while highly expressed core genes and tightly regulated TADs are mostly restricted within the slowly evolving A-compartment. In other organisms, the A/B compartments change depending on the cell life-stage (Falk et al., 2019). Within this context, our findings raise the intriguing possibility that similar changes also occur depending on the fungal and plant symbiotic status, and open avenues to identify the epigenetic mechanisms that generate and modify chromosome compartments during host-microbe interactions.

It will be now interesting to examine how this work extrapolates to AMF dikaryons, in particular how these strains compartmentalize their co-existing parental genomes and if these also significantly differ in gene content and size. Phasing parental genomes with high-quality Hi-C data is a requirement to fully address these questions, and determine how co-existing genomes regulate nuclear dynamics in these strains (Serghi *et al.*, 2021; Kokkoris *et al.*, 2021).

Acknowledgments

We thank Benjamin Schwessinger and Daniel Croll for their helpful comments on an earlier version of this manuscript, and Christophe Roux for providing information about publicly available, high-quality RNA-seq data. Our research is funded by the Discovery program of the Natural Sciences and Engineering Research Council (RGPIN2020-05643), a Discovery Accelerator Supplements Program (RGPAS-2020-00033). N.C. is a University of Ottawa Research Chair in Microbial Genomics. J.S. is supported by an Australian Research Council (ARC) Discovery Early Career Researcher Award (DE190100066), and E.C. and W.I. were

bioRxiv preprint doi: https://doi.org/10.1101/2021.08.12.456011; this version posted October 29, 2021. The copyright holder for this preprint (which was not certified by peer review) is the author/funder, who has granted bioRxiv a license to display the preprint in perpetuity. It is made available under aCC-BY-NC-ND 4.0 International license.

supported by JSPS Postdoctoral Fellowships for Research in Japan and JSPS KAKENHI Grant Number 19F19089.

Figure legends

Figure 1: Examples of variability in the size, and gene content and density between the homologous chromosomes of R. irregularis strains analyzed in this study. Red density plot shows gene density, and blue density plot shows repeat density. The colors of karyoplots indicate different strains. **A) Homologous chromosomes contain different rRNA operon copy numbers.** Chromosome 18 of C2 contains only four operon copies, whereas strain B3 carries six copies on the same chromosome. **B) Homologous chromosomes vary greatly in size**. Size difference between chromosome 8 of 4401 strain and chromosome 8 of DAOM197198 strain is over 1.1 Mb. **C) Chromosomes carrying MAT locus also vary in size.** C2 and 4401 strains carry the same MAT type, MAT6. However, chromosome sizes still differ by 700 kb.

Figure 2: Chromatin folding inside of the *R. irregularis* nucleus and visualization of intra- and inter-chromosomal physical interactions in Hi-C maps. **A) Schematic showing the compaction of chromatin fibers inside of a nucleus**. Chromatin fibers physically interact with each other and may fold into regions called compartments and topologically associated domains. **B) Hi-C contact maps showing the compartmentalization in the chromosome 1 of the *R. irregularis*.** In these heat maps, created to demonstrate contact frequencies throughout the genome, genome coordinates are represented on both axes. In an individual chromosome, regions that interact with each other result in an increase in contact frequencies and reveals the compartmentalized nature of the chromosome. These bright squares highlight increased contact frequency within and between chromosomes, are further analyzed to group them into euchromatin or heterochromatin compartments. Left: For chromosome l, the compartment shown in the red square belongs to compartment A, and is surrounded by two B-compartment regions shown in orange squares. Right: when the interactions of several chromosomes are analyzed, a “checkered” pattern indicates the genome arrangement of the euchromatin or heterochromatin compartments of *R. irregularis*. Telomeres are clearly visible in the Hi-C maps at the tip of each chromosome.

Figure 3: A/B compartments have different gene and repeat densities, and their genes contain different pfam domains. A) The two compartments carry significantly different

bioRxiv preprint doi: https://doi.org/10.1101/2021.08.12.456011; this version posted October 29, 2021. The copyright holder for this preprint (which was not certified by peer review) is the author/funder, who has granted bioRxiv a license to display the preprint in perpetuity. It is made available under aCC-BY-NC-ND 4.0 International license.

gene and repeat densities. The boxplots show the number of gene and repeats in 10kb intervals. T-test shows that compartment A has significantly higher gene density, and significantly lower repeat density compared to compartment B**. B) Gene numbers that carry specific Pfam domains also vary between compartments**. Circles highlight the total of number of genes carrying specific Pfam domains in located in compartment A (red circles) or B (blue circles), with the size of the circle being proportionate to the number of genes that carry that domain. Inter-strain variability in pfam domains is also evident within each compartment.

Figure 4: Gene expression and methylation analyses for the A/B compartments. T-test was conducted to show significance. **A) Genes in the A compartment show significantly higher expression levels measured in Transcripts Per Million (TPM) than genes in the B-compartment in all three conditions. B) Genes encoding secreted proteins are up-regulated in both in planta conditions in the B-compartment, but not in the A-compartment. a)** Compartment A shows significant upregulation of secreted proteins *in planta* Allium condition when compared to germinated spores. **b)** Compartment A does not show a significant secreted protein expression change when *in planta* Medicago expressions are compared to the expression of germinated spores. **c)** Compartment B shows significant upregulation of secreted proteins *in planta* Allium condition when compared to germinated spores. **d)** Compartment B shows significant upregulation of secreted proteins *in planta* Medicago condition when compared to germinated spores. **C) Gene median methylation frequencies of all methylated genes (methylation frequency median > 0) that are located in A/B compartments.** A compartment display significantly lower gene median methylation frequencies than the B compartment.

Supplemental figures and tables legends

Figure S1: *R. irregularis* C2, A1, B3 and 4401 strain chromosomes. The length of all 33 chromosomes is indicated in the karyoplots. Telomere repeats, MAT locus and small subunit rRNA locations are marked. Gene densities are shown in red, and repeat densities are shown in blue color.

Figure S2: Bubble plot showing 10 most abundant transposable elements and their distribution in five assemblies of *R. irregularis* strains.

bioRxiv preprint doi: https://doi.org/10.1101/2021.08.12.456011; this version posted October 29, 2021. The copyright holder for this preprint (which was not certified by peer review) is the author/funder, who has granted bioRxiv a license to display the preprint in perpetuity. It is made available under aCC-BY-NC-ND 4.0 International license.

Figure S3: Gene orthologies and Pfam domain numbers in five strains of *R. irregularis*. a) Protein orthologs of A1, B3, C2, DAOM-197198 and 4401 strains. **b) Pfam protein domain abundance comparison between five *R. irregularis* strains.** After the 100 most abundant Pfam protein domains were selected, the frequency values were transformed using a t-test. This way, relative enrichment (red) and relative depletion (blue) were shown.

Figure S4: Hierarchical clustering of *k*-mer distance estimations between chromosomes of the strains.

Figure S5: Heat map showing Hi-C contact frequencies between 33 chromosomes for strain DAOM-197198, C2, A1, B3 and 4401. Regions having higher contact frequencies are found in close contact in the nucleus, whereas regions having fewer contact frequencies are far away from each other.

Figure S6: Heat map showing Hi-C contact probabilities of individual chromosomes of strain DAOM-197198. Chromosomal regions having higher contact probabilities are found in close contact with each other, whereas regions having fewer contact probabilities are far away from each other. PCA eigenvectors were calculated for 10kb intervals and were plotted under the chromosome contact maps.

Figure S7: Heat map showing Hi-C contact probabilities of individual chromosomes of strain C2. Chromosomal regions having higher contact probabilities are found in close contact with each other, whereas regions having fewer contact probabilities are far away from each other. PCA eigenvectors were calculated for 10kb intervals and were plotted under the chromosome contact maps.

Figure S8: Heat map showing Hi-C contact probabilities of individual chromosomes of strain A1 Chromosomal regions having higher contact probabilities are found in close contact with each other, whereas regions having fewer contact probabilities are far away from each other. PCA eigenvectors were calculated for 10kb intervals and were plotted under the chromosome contact maps.

Figure S9: Heat map showing Hi-C contact probabilities of individual chromosomes of strain B3 Chromosomal regions having higher contact probabilities are found in close contact with each other, whereas regions having fewer contact probabilities are far away from each

bioRxiv preprint doi: https://doi.org/10.1101/2021.08.12.456011; this version posted October 29, 2021. The copyright holder for this preprint (which was not certified by peer review) is the author/funder, who has granted bioRxiv a license to display the preprint in perpetuity. It is made available under aCC-BY-NC-ND 4.0 International license.

other. PCA eigenvectors were calculated for 10kb intervals and were plotted under the chromosome contact maps.

Figure S10: Heat map showing Hi-C contact probabilities of individual chromosomes of strain 4401 Chromosomal regions having higher contact probabilities are found in close contact with each other, whereas regions having fewer contact probabilities are far away from each other. PCA eigenvectors were calculated for 10kb intervals and were plotted under the chromosome contact maps.

Figure S11: Strain-specific chromosomal differentiation events can be observed in Hi-C contact maps. Differentiation events that can be observed on contact maps and synteny plots were shown with an orange arrow. Repeat densities of the chromosomes are shown in blue color, and the synteny blocks are shown in purple. **a) Strain-specific repeat expansion found in chromosome 8 of strain 4401.** A) A repeat expansion event can be observed in chromosome 8 of 4401 strain, between regions 1Mb and 3Mb. As the same repeats get expanded, the contact of Hi-C reads in that region increase, leading to the increased brightness. B) Synteny blocks between chromosome 8 from DAOM-197198 and 4401 shows absence of synteny blocks in the repeat expansion region. In the regions showing no synteny between the two strains, DAOM-197198 strain has 157 genes and 1240 repeats whereas 4401 strain has 389 genes and 2799 repeats. **b) Strain specific inversion event in chromosome 18 of strain C2.** A) An inversion event can be observed in chromosome 18 of C2 strain, around 2Mb region. This differentiation event also causes an abnormality in the contact map around that region. B) Synteny blocks between chromosome 18 from DAOM-197198 and C2 show multiple inversion events. **c) Strain specific inversion event in chromosome 17 of strain A1.** A) An inversion event can be observed in chromosome 17 of A1 strain, before 1 Mb region. This differentiation event also causes an abnormality in the contact map around that region. B) Synteny blocks between chromosome 17 from DAOM-197198 and A1 show multiple inversion events. **d) Strain specific inversion event in chromosome 18 of strain B3.** A) An inversion event can be observed in chromosome 18 of B3 strain, around 2Mb region. This differentiation event also causes an abnormality in the contact map around that region. B) Synteny blocks between chromosome 18 from DAOM-197198 and B3 show multiple inversion events.

bioRxiv preprint doi: https://doi.org/10.1101/2021.08.12.456011; this version posted October 29, 2021. The copyright holder for this preprint (which was not certified by peer review) is the author/funder, who has granted bioRxiv a license to display the preprint in perpetuity. It is made available under aCC-BY-NC-ND 4.0 International license.

Figure S12: Distribution of core and dispensable genes in compartments A and B. Protein orthologs of A1, C2 and DAOM-197198 strains were identified with FastOrtho (Wattam *et al.*, 2014), using following parameters: 50% identity and 50% coverage. The genes were then grouped into A and B compartments. Core and core duplicated gene numbers were added up in each compartment to represent the "core group" count, and dispensable, specific and specific duplicated gene numbers were added up to make up the "dispensable group" count.

Figure S13: A) For each A/B compartment, the median methylation frequencies are collected and their distribution is plotted**.** The A compartment display higher median methylation frequencies than the B compartment. Highly methylated CpG sites (median methylation frequency > 80%) occur more frequently in the A compartment. **B)** CpG methylation frequencies of transposable elements in compartments A and B. Individual CpG methylation frequencies of transposable elements found in compartments A and B are shown as green dots. Methylation medians are shown as red dots.

Figure S14: Example of inversions in synteny blocks between chromosome 13 of DAOM-197198, C2 and A1 strains. The colors on the karyoplots represent the compartments. Compartment A is represented by blue color, whereas compartment B is represented by red color. Synteny blocks are created by MCScanx(Wang *et al.*, 2012), and inversions are highlighted. Orange links show inverted synteny blocks between DAOM-197198 and A1, and green links show inverted synteny blocks between DAOM-197198 and C2. Majority of the inversions are observed in compartment B.

Table S1: Location and number of ribosomal RNA operons within and across strains analyzed in this study.

Table S2: A/B compartment properties in the model strain DAOM-197198. The A-compartment is more gene-dense, while the B-compartment is more repeat-rich. However, the B-compartment has significantly more secreted proteins, candidate apoplastic effectors and candidate cytoplasmic effectors than the A-compartment (Fisher's exact test: * indicates $p < 0.05$).

bioRxiv preprint doi: https://doi.org/10.1101/2021.08.12.456011; this version posted October 29, 2021. The copyright holder for this preprint (which was not certified by peer review) is the author/funder, who has granted bioRxiv a license to display the preprint in perpetuity. It is made available under aCC-BY-NC-ND 4.0 International license.

Table S3: Comparison of A and B compartment similarity in DAOM-197198, C2 and A1 strains. Overall, A compartment is more conserved with higher similarity between strains compared to B compartment.

References

Arima Genomics. **2019**. 01_mapping_arima.sh.

Badet T, Oggenfuss U, Abraham L, McDonald BA, Croll D. **2020**. A 19-isolate reference-quality global pangenome for the fungal wheat pathogen Zymoseptoria tritici. *BMC Biology* **18**.

Bertazzoni S, Williams AH, Jones DA, Syme RA, Tan K-C, Hane JK. **2018**. Accessories Make the Outfit: Accessory Chromosomes and Other Dispensable DNA Regions in Plant-Pathogenic Fungi. *Molecular Plant-Microbe Interactions®* **31**: 779–788.

Bonfante P, Anca IA. **2009**. Plants, mycorrhizal fungi, and bacteria: A network of interactions. *Annual Review of Microbiology* **63**: 363–383.

Bruns TD, Corradi N, Redecker D, Taylor JW, Öpik M. **2018**. Glomeromycotina: what is a species and why should we care? *New Phytologist* **220**: 963–967.

Chen ECCH, Mathieu S, Sedzielewska-Toro K, Peart M, Pelin A, Ndikumana S, Ropars J, Dreissig S, Fuchs J, Brachmann A, *et al.* 2018a. Single nucleus sequencing reveals evidence of inter-nucleus recombination in arbuscular mycorrhizal fungi. *eLife* **8**.

Chen ECH, Morin E, Beaudet D, Noel J, Yildirir G, Ndikumana S, Charron P, St-Onge C, Giorgi J, Krüger M, *et al.* 2018b. High intraspecific genome diversity in the model arbuscular mycorrhizal symbiont *Rhizophagus irregularis*. *New Phytologist* **220**: 1161–1171.

Corradi N, Bonfante P. **2012**. The Arbuscular Mycorrhizal Symbiosis: Origin and Evolution of a Beneficial Plant Infection (J Heitman, Ed.). *PLoS Pathogens* **8**: e1002600.

Corradi N, Brachmann A. **2017**. *Fungal Mating in the Most Widespread Plant Symbionts?* Elsevier.

Corradi N, Croll D, Colard A, Kuhn G, Ehinger M, Sanders IR. **2007**. Gene copy number polymorphisms in an arbuscular mycorrhizal fungal population. *Applied and Environmental Microbiology* **73**: 366–369.

Corradi N, Hijri M, Fumagalli L, Sanders IR. **2004**. Arbuscular mycorrhizal fungi (Glomeromycota) harbour ancient fungal tubulin genes that resemble those of the chytrids (Chytridiomycota). *Fungal Genetics and Biology* **41**: 1037–1045.

Dallaire AA. **2021**. Transcriptional activity and epigenetic regulation of transposable ele-ments in the symbiotic fungus *Rhizophagus irregularis*. *bioRxiv*: 2021.03.30.436303.

Dekker J, Heard E. **2015**. Structural and functional diversity of Topologically Associating Domains. *FEBS Letters* **589**: 2877–2884.

bioRxiv preprint doi: https://doi.org/10.1101/2021.08.12.456011; this version posted October 29, 2021. The copyright holder for this preprint (which was not certified by peer review) is the author/funder, who has granted bioRxiv a license to display the preprint in perpetuity. It is made available under aCC-BY-NC-ND 4.0 International license.

Delaux PM, Schornack S. **2021**. Plant evolution driven by interactions with symbiotic and pathogenic microbes. *Science* **371**.

Denton JF, Lugo-Martinez J, Tucker AE, Schrider DR, Warren WC, Hahn MW. **2014**. Extensive Error in the Number of Genes Inferred from Draft Genome Assemblies. *PLoS Computational Biology* **10**.

El-Gebali S, Mistry J, Bateman A, Eddy SR, Luciani A, Potter SC, Qureshi M, Richardson LJ, Salazar GA, Smart A, *et al.* 2019. The Pfam protein families database in 2019. *Nucleic Acids Research* **47**: D427–D432.

Falk M, Feodorova Y, Naumova N, Imakaev M, Lajoie BR, Leonhardt H, Joffe B, Dekker J, Fudenberg G, Solovei I, *et al.* 2019. Heterochromatin drives compartmentalization of inverted and conventional nuclei. *Nature* **570**.

Flynn JM, Hubley R, Goubert C, Rosen J, Clark AG, Feschotte C, Smit AF. **2020**. RepeatModeler2 for automated genomic discovery of transposable element families. *Proceedings of the National Academy of Sciences of the United States of America* **117**: 9451–9457.

Fortin J-P, Hansen KD. **2015**. Reconstructing A/B compartments as revealed by Hi-C using long-range correlations in epigenetic data. *Genome Biology 2015 16:1* **16**: 1–23.

Frantzeskakis L, Kusch S, Panstruga R. **2019**. The need for speed: compartmentalized genome evolution in filamentous phytopathogens. *Molecular Plant Pathology* **20**: 3–7.

Galazka JM, Klocko AD, Uesaka M, Honda S, Selker EU, Freitag M. **2016**. Neurospora chromosomes are organized by blocks of importin alpha-dependent heterochromatin that are largely independent of H3K9me3. *Genome Research* **26**: 1069–1080.

Garmaroodi HS, Taga M. **2007**. Duplication of a conditionally dispensable chromosome carrying pea pathogenicity (PEP) gene clusters in Nectria haematococca. *Molecular Plant-Microbe Interactions* **20**: 1495–1504.

Gel B, Serra E. **2017**. KaryoploteR: An R/Bioconductor package to plot customizable genomes displaying arbitrary data. *Bioinformatics* **33**: 3088–3090.

Ghurye J, Pop M, Koren S, Bickhart D, Chin CS. **2017**. Scaffolding of long read assemblies using long range contact information. *BMC Genomics* **18**: 527.

Ghurye J, Rhie A, Walenz BP, Schmitt A, Selvaraj S, Pop M, Phillippy AM, Koren S. **2019**. Integrating Hi-C links with assembly graphs for chromosome-scale assembly. *PLoS Computational Biology* **15**: e1007273.

Hancock JM, Bishop MJ. **2004**. HMMer. In: Dictionary of Bioinformatics and Computational Biology. Chichester, UK: John Wiley & Sons, Ltd.

Jerković I, Szabo Q, Bantignies F, Cavalli G. **2020**. Higher-Order Chromosomal Structures Mediate Genome Function. *Journal of Molecular Biology* **432**: 676–681.

bioRxiv preprint doi: https://doi.org/10.1101/2021.08.12.456011; this version posted October 29, 2021. The copyright holder for this preprint (which was not certified by peer review) is the author/funder, who has granted bioRxiv a license to display the preprint in perpetuity. It is made available under aCC-BY-NC-ND 4.0 International license.

Kamel L, Tang N, Malbreil M, San Clemente H, Le Marquer M, Roux C, dit Frey NF. **2017**. The comparison of expressed candidate secreted proteins from two arbuscular mycorrhizal fungi unravels common and specific molecular tools to invade different host plants. *Frontiers in Plant Science* **8**.

Kempfer R, Pombo A. **2020**. Methods for mapping 3D chromosome architecture. *Nature Reviews Genetics* **21**: 207–226.

Kim S, Liachko I, Brickner DG, Cook K, Noble WS, Brickner JH, Shendure J, Dunham MJ. **2017**. The dynamic three-dimensional organization of the diploid yeast genome. *eLife* **6**.

Kloppholz S, Kuhn H, Requena N. **2011**. A secreted fungal effector of glomus intraradices promotes symbiotic biotrophy. *Current Biology* **21**: 1204–1209.

Koch AM, Kuhn G, Fontanillas P, Fumagalli L, Goudet J, Sanders IR. **2004**. High genetic variability and low local diversity in a population of arbuscular mycorrhizal fungi. *Proceedings of the National Academy of Sciences of the United States of America* **101**: 2369–2374.

Kokkoris V, Chagnon PL, Yildirir G, Clarke K, Goh D, MacLean AM, Dettman J, Stefani F, Corradi N. **2021**. Host identity influences nuclear dynamics in arbuscular mycorrhizal fungi. *Current Biology* **31**: 1531-1538.e6.

Kokkoris V, Stefani F, Dalpé Y, Dettman J, Corradi N. **2020**. Nuclear Dynamics in the Arbuscular Mycorrhizal Fungi. *Trends in Plant Science* **25**: 765–778.

Koren S, Walenz BP, Berlin K, Miller JR, Bergman NH, Phillippy AM. **2017**. Canu: Scalable and accurate long-read assembly via adaptive κ-mer weighting and repeat separation. *Genome Research* **27**: 722–736.

Krogh A, Larsson B, Von Heijne G, Sonnhammer ELL. **2001**. Predicting transmembrane protein topology with a hidden Markov model: Application to complete genomes. *Journal of Molecular Biology* **305**: 567–580.

Kurtz S, Phillippy A, Delcher AL, Smoot M, Shumway M, Antonescu C, Salzberg SL. **2004**. Versatile and open software for comparing large genomes. *Genome biology* **5**: 12.

Lea AJ, Vockley CM, Johnston RA, Del Carpio CA, Barreiro LB, Reddy TE, Tung J. **2018**. Genome-wide quantification of the effects of DNA methylation on human gene regulation. *eLife* **7**.

Li H. **2013**. Aligning sequence reads, clone sequences and assembly contigs with BWA-MEM.

Li W, Cowley A, Uludag M, Gur T, McWilliam H, Squizzato S, Park YM, Buso N, Lopez R. **2015**. The EMBL-EBI bioinformatics web and programmatic tools framework. *Nucleic Acids Research* **43**: W580–W584.

Li X, Huang X, Chen G, Zou L, Wei L, Hua J. **2018**. Complete genome sequence of the sesame pathogen Ralstonia solanacearum strain SEPPX 05. *Genes and Genomics* **40**: 657–668.

bioRxiv preprint doi: https://doi.org/10.1101/2021.08.12.456011; this version posted October 29, 2021. The copyright holder for this preprint (which was not certified by peer review) is the author/funder, who has granted bioRxiv a license to display the preprint in perpetuity. It is made available under aCC-BY-NC-ND 4.0 International license.

Lin K, Limpens E, Zhang Z, Ivanov S, Saunders DGO, Mu D, Pang E, Cao H, Cha H, Lin T, *et al.* 2014. Single Nucleus Genome Sequencing Reveals High Similarity among Nuclei of an Endomycorrhizal Fungus. *PLoS Genetics* **10**.

Love MI, Huber W, Anders S. **2014**. Moderated estimation of fold change and dispersion for RNA-seq data with DESeq2. *Genome Biology* **15**: 550.

Lutzoni F, Nowak MD, Alfaro ME, Reeb V, Miadlikowska J, Krug M, Arnold AE, Lewis LA, Swofford DL, Hibbett D, *et al.* 2018. Contemporaneous radiations of fungi and plants linked to symbiosis. *Nature Communications* **9**: 1–11.

Maeda T, Kobayashi Y, Kameoka H, Okuma N, Takeda N, Yamaguchi K, Bino T, Shigenobu S, Kawaguchi M. **2018**. Evidence of non-tandemly repeated rDNAs and their intragenomic heterogeneity in *Rhizophagus irregularis*. *Communications Biology* **1**.

Malar MC, Krüger M, Krüger C, Wang Y, Stajich JE, Keller J, Chen ECH, Yildirir G, Villeneuve-Laroche M, Roux C, *et al.* 2021a. The genome of Geosiphon pyriformis reveals ancestral traits linked to the emergence of the arbuscular mycorrhizal symbiosis. *Current Biology* **31**: 1570-1577.e4.

Malar MC, Roux C, Corradi N. **2021b**. Regulation of mating genes during arbuscular mycorrhizal isolate co-existence—where is the evidence? *The ISME Journal 2021 15:8* **15**: 2173–2179.

Marçais G, Delcher AL, Phillippy AM, Coston R, Salzberg SL, Zimin A. **2018**. MUMmer4: A fast and versatile genome alignment system. *PLoS Computational Biology* **14**.

Martin FM, Uroz S, Barker DG. **2017**. Ancestral alliances: Plant mutualistic symbioses with fungi and bacteria. *Science* **356**.

Mathieu S, Cusant L, Roux C, Corradi N. **2018a**. Arbuscular mycorrhizal fungi: intraspecific diversity and pangenomes. *New Phytologist* **220**: 1129–1134.

McCarthy CGP, Fitzpatrick DA. **2019**. Pan-genome analyses of model fungal species. *Microbial Genomics* **5**.

Montoliu-Nerin M, Sánchez-García M, Bergin C, Grabherr M, Ellis B, Kutschera VE, Kierczak M, Johannesson H, Rosling A. **2020**. Building de novo reference genome assemblies of complex eukaryotic microorganisms from single nuclei. *Scientific Reports* **10**.

Morin E, Miyauchi S, San Clemente H, Chen ECH, Pelin A, de la Providencia I, Ndikumana S, Beaudet D, Hainaut M, Drula E, *et al.* 2019. Comparative genomics of *Rhizophagus irregularis*, *R. cerebriforme*, *R. diaphanus* and *Gigaspora rosea* highlights specific genetic features in Glomeromycotina. *New Phytologist* **222**: 1584–1598.

Ondov BD, Treangen TJ, Melsted P, Mallonee AB, Bergman NH, Koren S, Phillippy AM. **2016**. Mash: Fast genome and metagenome distance estimation using MinHash. *Genome Biology* **17**: 1–14.

bioRxiv preprint doi: https://doi.org/10.1101/2021.08.12.456011; this version posted October 29, 2021. The copyright holder for this preprint (which was not certified by peer review) is the author/funder, who has granted bioRxiv a license to display the preprint in perpetuity. It is made available under aCC-BY-NC-ND 4.0 International license.

Patro R, Duggal G, Love MI, Irizarry RA, Kingsford C. **2017**. Salmon provides fast and bias-aware quantification of transcript expression. *Nature Methods* **14**: 417–419.

Petersen TN, Brunak S, Von Heijne G, Nielsen H. **2011**. SignalP 4.0: Discriminating signal peptides from transmembrane regions. *Nature Methods* **8**: 785–786.

Plett JM, Martin F. **2012**. Poplar root exudates contain compounds that induce the expression of MiSSP7 in Laccaria bicolor. *Plant Signaling and Behavior* **7**.

Pombo A, Dillon N. **2015**. Three-dimensional genome architecture: Players and mechanisms. *Nature Reviews Molecular Cell Biology* **16**: 245–257.

Quinlan AR, Hall IM. **2010**. BEDTools: A flexible suite of utilities for comparing genomic features. *Bioinformatics* **26**: 841–842.

Ramírez F, Bhardwaj V, Arrigoni L, Lam KC, Grüning BA, Villaveces J, Habermann B, Akhtar A, Manke T. **2018**. High-resolution TADs reveal DNA sequences underlying genome organization in flies. *Nature Communications* **9**: 1–15.

Reinhardt D, Roux C, Corradi N, Di Pietro A. **2021**. Lineage-Specific Genes and Cryptic Sex: Parallels and Differences between Arbuscular Mycorrhizal Fungi and Fungal Pathogens. *Trends in Plant Science* **26**: 111–123.

Riley R, Charron P, Idnurm A, Farinelli L, Dalpé Y, Martin F, Corradi N. **2014**. Extreme diversification of the mating type-high-mobility group (MATA-HMG) gene family in a plant-associated arbuscular mycorrhizal fungus. *New Phytologist* **201**: 254–268.

Roach MJ, Schmidt SA, Borneman AR. **2018**. Purge Haplotigs: Allelic contig reassignment for third-gen diploid genome assemblies. *BMC Bioinformatics* **19**: 1–10.

Ropars J, Toro KSS, Noel J, Pelin A, Charron P, Farinelli L, Marton T, Krüger M, Fuchs J, Brachmann A, *et al.* 2016. Evidence for the sexual origin of heterokaryosis in arbuscular mycorrhizal fungi. *Nature Microbiology* **1**: 16033.

Savary R, Masclaux FG, Wyss T, Droh G, Cruz Corella J, Machado AP, Morton JB, Sanders IR. **2018**. A population genomics approach shows widespread geographical distribution of cryptic genomic forms of the symbiotic fungus *Rhizophagus irregularis*. *ISME Journal* **12**: 17–30.

Schmitt AD, Hu M, Ren B. **2016**. Genome-wide mapping and analysis of chromosome architecture. *Nature Reviews Molecular Cell Biology* **17**: 743–755.

Schwessinger B. **2016**. High quality DNA from Fungi for long read sequencing e.g. Pacbio. *Protocols.io*: 1–6.

Serghi EU, Kokkoris V, Cornell C, Dettman J, Stefani F, Corradi N. **2021**. Homo- and Dikaryons of the Arbuscular Mycorrhizal Fungus *Rhizophagus irregularis* Differ in Life History Strategy. *Frontiers in Plant Science* **12**: 1544.

bioRxiv preprint doi: https://doi.org/10.1101/2021.08.12.456011; this version posted October 29, 2021. The copyright holder for this preprint (which was not certified by peer review) is the author/funder, who has granted bioRxiv a license to display the preprint in perpetuity. It is made available under aCC-BY-NC-ND 4.0 International license.

Servant N, Varoquaux N, Lajoie BR, Viara E, Chen CJ, Vert JP, Heard E, Dekker J, Barillot E. **2015**. HiC-Pro: An optimized and flexible pipeline for Hi-C data processing. *Genome Biology* **16**.

Simão FA, Waterhouse RM, Ioannidis P, Kriventseva E V., Zdobnov EM. **2015**. BUSCO: Assessing genome assembly and annotation completeness with single-copy orthologs. *Bioinformatics* **31**: 3210–3212.

Smit AFA, Hubley R, Green P. No Title. *RepeatMasker Open-4.0.*

Soyer JL, El Ghalid M, Glaser N, Ollivier B, Linglin J, Grandaubert J, Balesdent MH, Connolly LR, Freitag M, Rouxel T, *et al.* 2014. Epigenetic Control of Effector Gene Expression in the Plant Pathogenic Fungus Leptosphaeria maculans. *PLoS Genetics* **10**: e1004227.

Spatafora JW, Chang Y, Benny GL, Lazarus K, Smith ME, Berbee ML, Bonito G, Corradi N, Grigoriev I, Gryganskyi A, *et al.* 2016. A phylum-level phylogenetic classification of zygomycete fungi based on genome-scale data. *Mycologia* **108**: 1028–1046.

Sperschneider J, Dodds PN. **2021**. EffectorP 3.0: prediction of apoplastic and cytoplasmic effectors in fungi and oomycetes. *bioRxiv*: 454080.

Sperschneider J, Jones AW, Nasim J, Xu B, Jacques S, Zhong C, Upadhyaya NM, Mago R, Hu Y, Figueroa M, *et al.* 2021. The stem rust fungus Puccinia graminis f. sp. tritici induces centromeric small RNAs during late infection that are associated with genome-wide DNA methylation. *BMC Biology 2021 19:1* **19**: 1–25.

Spielmann M, Lupiáñez DG, Mundlos S. **2018**. Structural variation in the 3D genome. *Nature Reviews Genetics* **19**: 453–467.

Stockinger H, Walker C, Schüßler A. **2009**. "Glomus intraradices DAOM197198", a model fungus in arbuscular mycorrhiza research, is not Glomus intraradices. *New Phytologist* **183**: 1176–1187.

Szabo Q, Bantignies F, Cavalli G. **2019**. Principles of genome folding into topologically associating domains. *Science Advances* **5**.

Tisserant E, Malbreil M, Kuo A, Kohler A, Symeonidi A, Balestrini R, Charron P, Duensing N, Frei Dit Frey N, Gianinazzi-Pearson V, *et al.* 2013. Genome of an arbuscular mycorrhizal fungus provides insight into the oldest plant symbiosis. *Proceedings of the National Academy of Sciences of the United States of America* **110**: 20117–20122.

Torres DE, Oggenfuss U, Croll D, Seidl MF. **2020**. Genome evolution in fungal plant pathogens: looking beyond the two-speed genome model. *Fungal Biology Reviews* **34**: 136–143.

Vaser R, Sović I, Nagarajan N, Šikić M. **2017**. Fast and accurate de novo genome assembly from long uncorrected reads. *Genome Research* **27**: 737–746.

bioRxiv preprint doi: https://doi.org/10.1101/2021.08.12.456011; this version posted October 29, 2021. The copyright holder for this preprint (which was not certified by peer review) is the author/funder, who has granted bioRxiv a license to display the preprint in perpetuity. It is made available under aCC-BY-NC-ND 4.0 International license.

Vlaardingerbroek I, Beerens B, Schmidt SM, Cornelissen BJC, Rep M. **2016**. Dispensable chromosomes in Fusarium oxysporum f. Sp. lycopersici. *Molecular Plant Pathology* **17**: 1455–1466.

Walker BJ, Abeel T, Shea T, Priest M, Abouelliel A, Sakthikumar S, Cuomo CA, Zeng Q, Wortman J, Young SK, *et al.* 2014. Pilon: An integrated tool for comprehensive microbial variant detection and genome assembly improvement. *PLoS ONE* **9**: 112963.

Wang Y, Tang H, Debarry JD, Tan X, Li J, Wang X, Lee TH, Jin H, Marler B, Guo H, *et al.* 2012. MCScanX: A toolkit for detection and evolutionary analysis of gene synteny and collinearity. *Nucleic Acids Research* **40**: e49.

Wattam AR, Abraham D, Dalay O, Disz TL, Driscoll T, Gabbard JL, Gillespie JJ, Gough R, Hix D, Kenyon R, *et al.* 2014. PATRIC, the bacterial bioinformatics database and analysis resource. *Nucleic Acids Research* **42**: D581.

Winter DJ, Ganley ARD, Young CA, Liachko I, Schardl CL, Dupont PY, Berry D, Ram A, Scott B, Cox MP. **2018**. Repeat elements organise 3D genome structure and mediate transcription in the filamentous fungus Epichloë festucae. *PLoS Genetics* **14**.

Wolff J, Bhardwaj V, Nothjunge S, Richard G, Renschler G, Gilsbach R, Manke T, Backofen R, Ramírez F, Grüning BA. **2018**. Galaxy HiCExplorer: A web server for reproducible Hi-C data analysis, quality control and visualization. *Nucleic Acids Research* **46**: W11–W16.

Wolff J, Rabbani L, Gilsbach R, Richard G, Manke T, Backofen R, Grüning BA. **2020**. Galaxy HiCExplorer 3: A web server for reproducible Hi-C, capture Hi-C and single-cell Hi-C data analysis, quality control and visualization. *Nucleic Acids Research* **48**: W177–W184.

Zeng T, Holmer R, Hontelez J, te Lintel-Hekkert B, Marufu L, de Zeeuw T, Wu F, Schijlen E, Bisseling T, Limpens E. **2018**. Host- and stage-dependent secretome of the arbuscular mycorrhizal fungus *Rhizophagus irregularis*. *Plant Journal* **94**: 411–425.

Zheng H, Xie W. **2019**. The role of 3D genome organization in development and cell differentiation. *Nature Reviews Molecular Cell Biology* **20**: 535–550.

Table 1 : *R. irregularis* strains genome assembly and annotation statistics

	DAOM197198	**A1**	**B3**	**C2**	**4401**
Chromosome-scale scaffolds					
Total size	147.2 Mb	147.1 Mb	146.8 Mb	161.9 Mb	146.8 Mb
# of scaffolds	33	33	33	33	33
BUSCO	96%	96%	96%	96.5%	96.5%

bioRxiv preprint doi: https://doi.org/10.1101/2021.08.12.456011; this version posted October 29, 2021. The copyright holder for this preprint (which was not certified by peer review) is the author/funder, who has granted bioRxiv a license to display the preprint in perpetuity. It is made available under aCC-BY-NC-ND 4.0 International license.

completeness					
Repeat content	49.05%	49.00%	50%	54.87%	48.07%
Number of genes	26,634	23,988	23,988	25,634	24,069
GC content	27.82%	27.78%	27.81%	28.23%	27.81%
Unplaced contigs					
Total size	2.6 Mb	0.5 Mb	1.3 Mb	0.4 Mb	0.9 Mb
# of contigs	104	29	42	12	25
Assembly N/L50	29/31.4 Kb	7/25.5 Kb	12/36.5 Kb	4/50.8 Kb	7/45.7 Kb

768

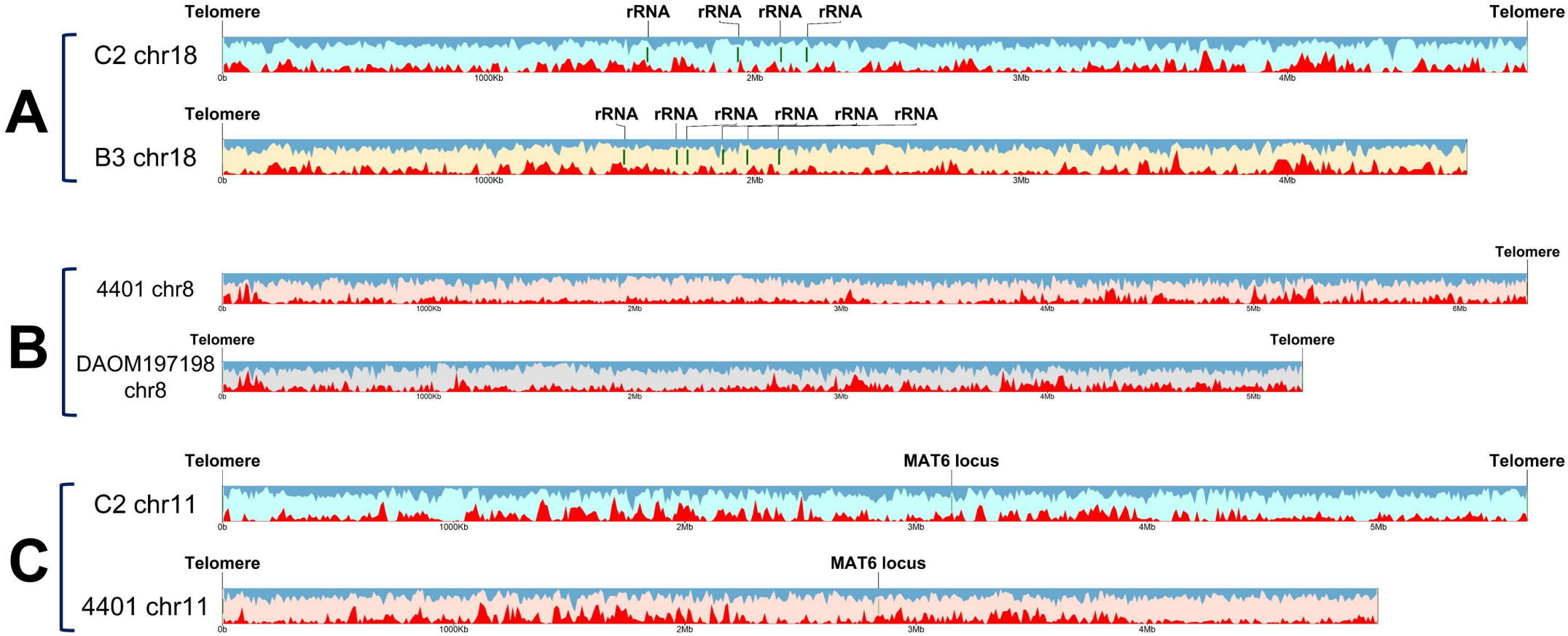
A
C2 chr18
Telomere
rRNA
rRNA
rRNA
rRNA
Telomere
0b
1000Kb
2Mb
3Mb
4Mb
B3 chr18
Telomere
rRNA
rRNA
rRNA
rRNA
rRNA
rRNA
0b
1000Kb
2Mb
3Mb
4Mb
B
4401 chr8
Telomere
0b
1000Kb
2Mb
3Mb
4Mb
5Mb
6Mb
DAOM197198 chr8
Telomere
Telomere
0b
1000Kb
2Mb
3Mb
4Mb
5Mb
C
C2 chr11
Telomere
MAT6 locus
Telomere
0b
1000Kb
2Mb
3Mb
4Mb
5Mb
4401 chr11
Telomere
MAT6 locus
0b
1000Kb
2Mb
3Mb
4Mb

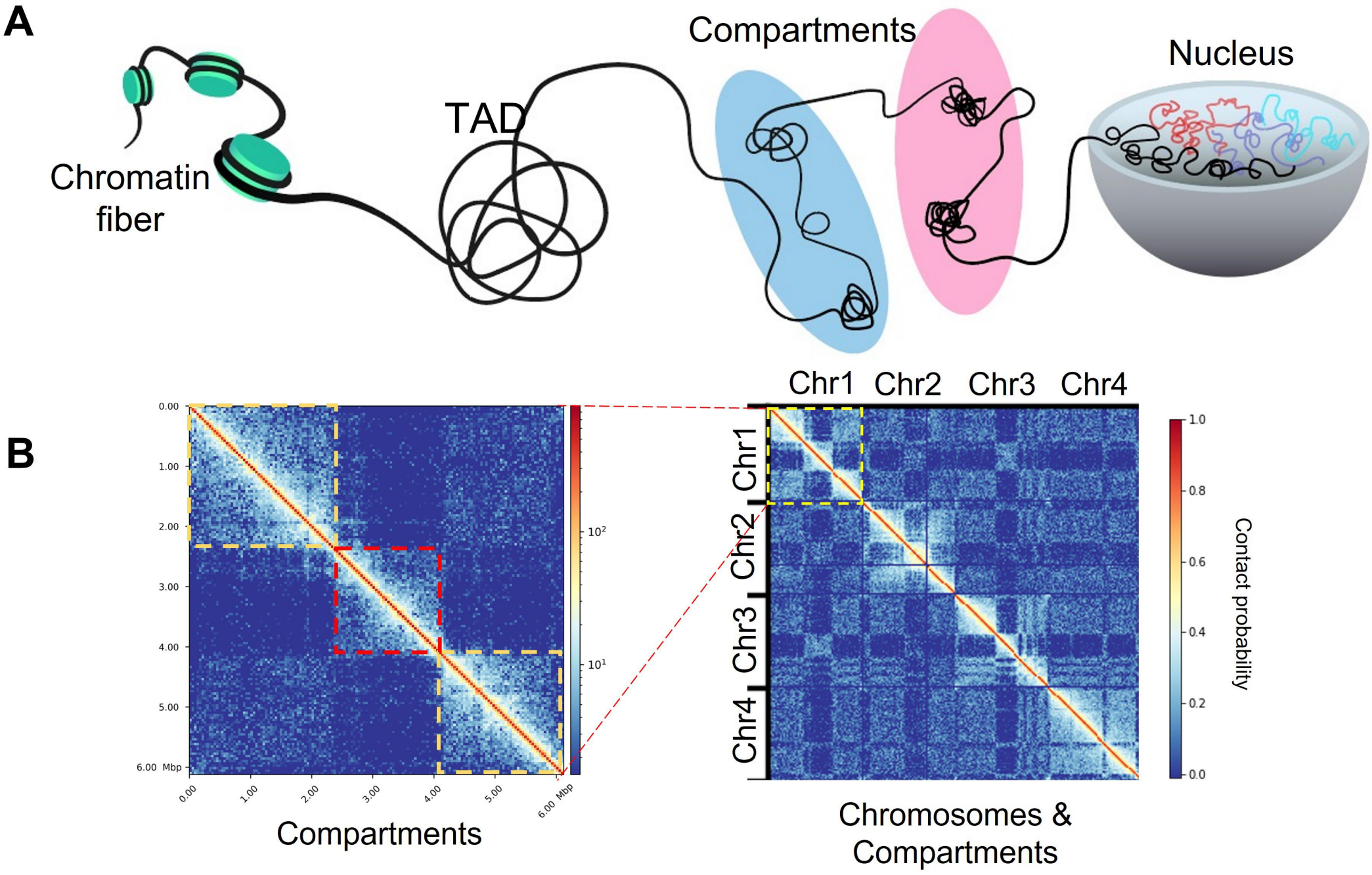
A
Chromatin fiber
TAD
Compartments
Nucleus
B
0.00
1.00
2.00
3.00
4.00
5.00
6.00 Mbp
Compartments
Chr1
Chr2
Chr3
Chr4
Chromosomes & Compartments
Contact probability
1.0
0.8
0.6
0.4
0.2
0.0

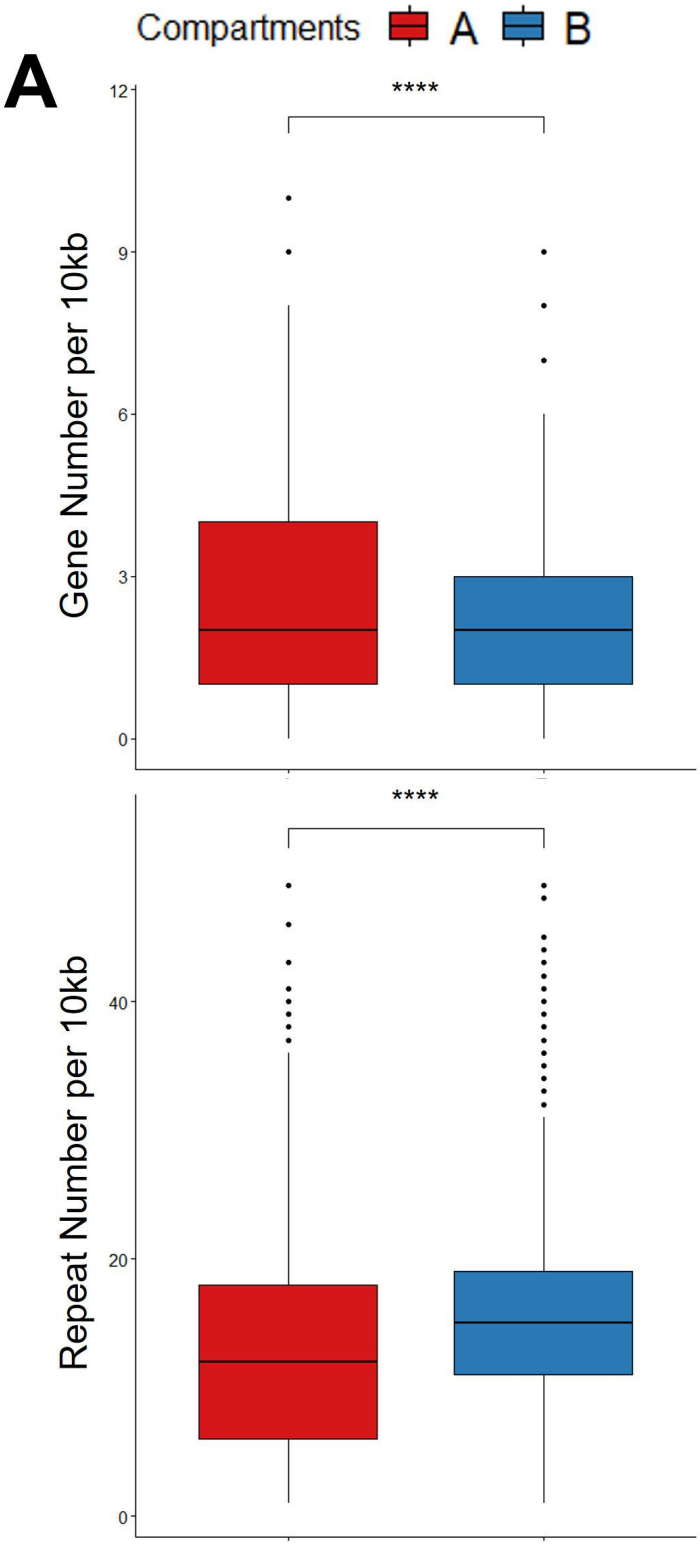
Compartments
A
B
A
****
Gene Number per 10kb
12
9
6
3
0
****
Repeat Number per 10kb
40
20
0

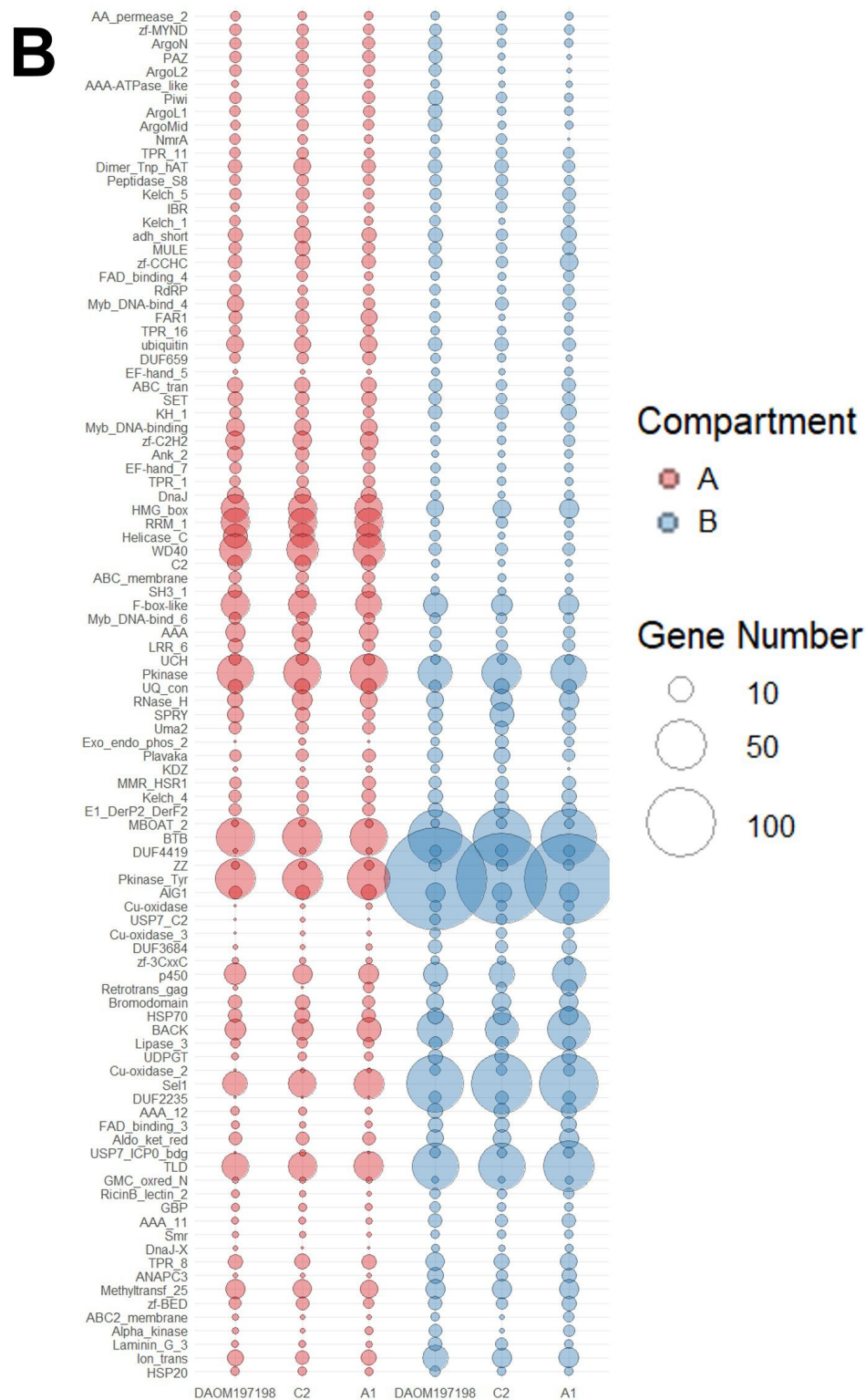
B
AA_permease_2
zf-MYND
ArgoN
PAZ
ArgoL2
AAA-ATPase_like
Piwi
ArgoL1
ArgoMid
NmrA
TPR_11
Dimer_Tnp_hAT
Peptidase_S8
Kelch_5
IBR
Kelch_1
adh_short
MULE
zf-CCHC
FAD_binding_4
RdRP
Myb_DNA-bind_4
FAR1
TPR_16
ubiquitin
DUF659
EF-hand_5
ABC_tran
SET
KH_1
Myb_DNA-binding
zf-C2H2
Ank_2
EF-hand_7
TPR_1
DnaJ
HMG_box
RRM_1
Helicase_C
WD40
C2
ABC_membrane
SH3_1
F-box-like
Myb_DNA-bind_6
AAA
LRR_6
UCH
Pkinase
UQ_con
RNase_H
SPRY
Uma2
Exo_endo_phos_2
Plavaka
KDZ
MMR_HSR1
Kelch_4
E1_DerP2_DerF2
MBOAT_2
BTB
DUF4419
ZZ
Pkinase_Tyr
AIG1
Cu-oxidase
USP7_C2
Cu-oxidase_3
DUF3684
zf-3CxxC
p450
Retrotrans_gag
Bromodomain
HSP70
BACK
Lipase_3
UDPGT
Cu-oxidase_2
Sel1
DUF2235
AAA_12
FAD_binding_3
Aldo_ket_red
USP7_ICP0_bdg
TLD
GMC_oxred_N
RicinB_lectin_2
GBP
AAA_11
Smr
DnaJ-X
TPR_8
ANAPC3
Methyltransf_25
zf-BED
ABC2_membrane
Alpha_kinase
Laminin_G_3
Ion_trans
HSP20
DAOM197198
C2
A1
DAOM197198
C2
A1
Compartment
A
B
Gene Number
10
50
100

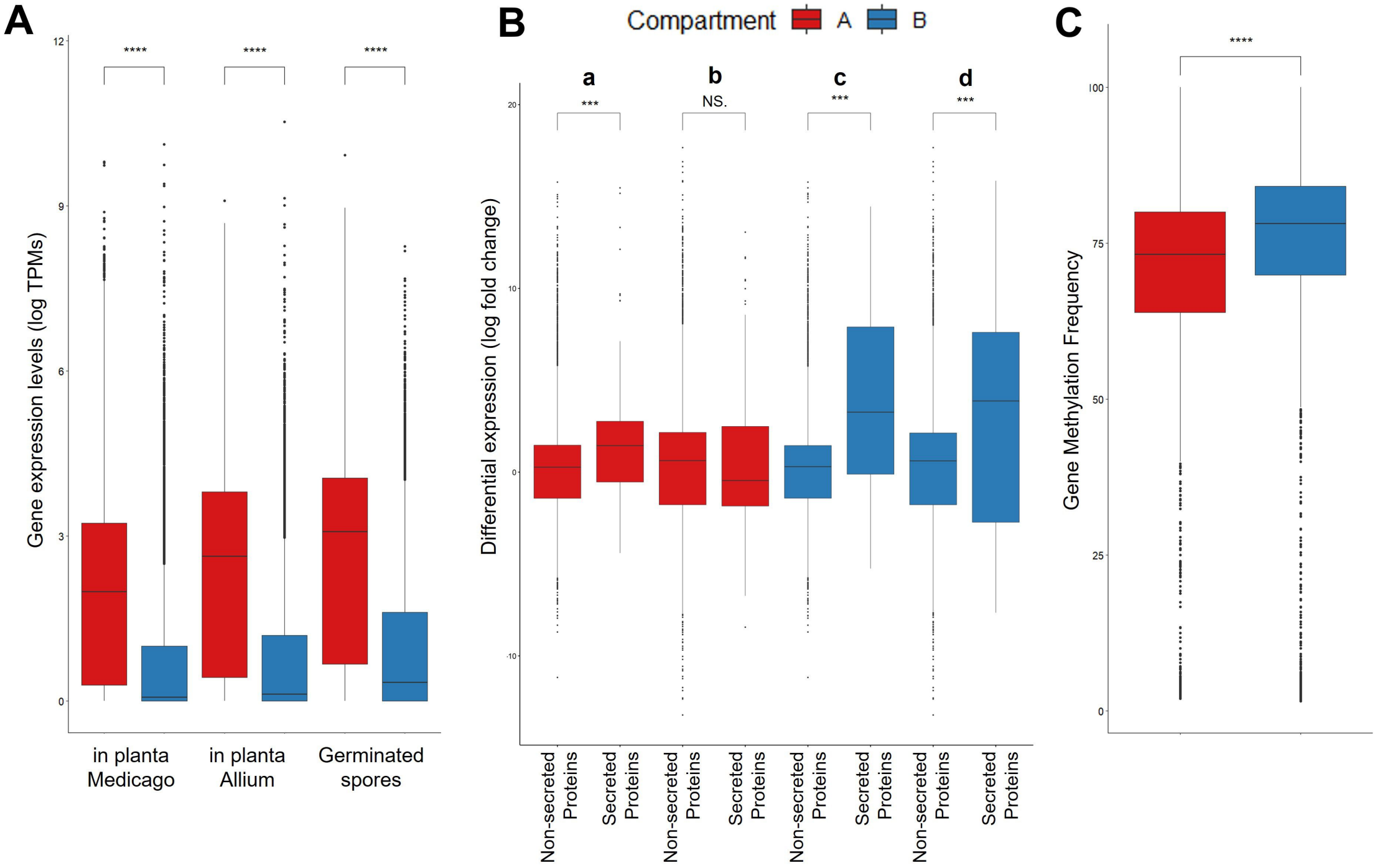
A
Gene expression levels (log TPMs)
12
9
6
3
0
****
****
****
in planta Medicago
in planta Allium
Germinated spores
B
Compartment
A
B
Differential expression (log fold change)
20
10
0
-10
a
b
c
d
***
NS.
***
***
Non-secreted Proteins
Secreted Proteins
Non-secreted Proteins
Secreted Proteins
Non-secreted Proteins
Secreted Proteins
Non-secreted Proteins
Secreted Proteins
C
Gene Methylation Frequency
100
75
50
25
0
****